Modelling the Gas Outflows in Quasars

A Thesis

submitted to
Indian Institute of Science Education and Research Pune in partial fulfilment of
the requirements for the BS-MS Dual Degree Programme
by

Oddharak Tyagi

Indian Institute of Science Education and Research Pune
Dr. Homi Bhabha Road,
Pashan, Pune 411008, INDIA.

April, 2020
Supervisor: R. Srianand
Oddharak Tyagi

Certificate

This is to certify that this dissertation entitled Modelling the Gas Outflows in Quasars towards the partial fulfilment of the BS-MS dual degree programme at the Indian Institute of Science Education and Research, Pune represents study/work carried out by Oddharak Tyagi at Inter-University Centre for Astronomy and Astrophysics, Pune under the supervision of R. Srianand, during the academic year 2019-2020.

R. Srianand

Committee:

R. Srianand

P. Subramanian

Declaration

I hereby declare that the matter embodied in the report entitled Modelling the Gas Outflows in Quasars are the results of the work carried out by me at the Inter-University Centre for Astronomy and Astrophysics, Pune, under the supervision of R. Srianand and the same has not been submitted elsewhere for any other degree.

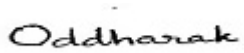

Oddharak Tyagi
Date : 10/04/2020

Contents

List of Figures

List of Tables

1 Abstract

The existence of high velocity outflows from quasars is confirmed by the presence of blue-shifted absorption signatures in the spectrum of quasars. Hints towards the origin and nature of these outflows are essential to our understanding of the dynamics of gas in the central regions of the active galactic nucleus but also of the metal enrichment of intergalactic space. It has been suggested that these outflows are accelerated by line radiation absorption and thus might exhibit line-locking. One possible way to investigate this claim is by looking for the presence of absorption features with velocity separation similar to doublet splittings of C IV, O VI and N V. In this work I construct photo-ionization grids using the software CLOUDY to model an associated absorption system in a quasar atmosphere and obtained the equilibrium solutions between radiative acceleration due to resonance line absorption and gravitational acceleration due to the central super-massive black hole. To test the predictions of the model I looked at the spectra of a line-locked quasar Q1511+09 at three different epochs to put bounds on the acceleration of these line-locked systems. The column densities for these clouds was estimated using the apparent optical depth method and finally the predictions of the model were compared to the observations to conclude that O VI doublet plays the dominant role in locking and that it is very unlikely that steady state line locking takes place.

2 Introduction

Radiation emitted by quasars reaches our detectors after passing through a lot of material that lies along the line of sight. Information about the nature and amount of the intervening material can be inferred by studying the characteristic imprints that these interactions leave on the quasar spectrum we observe. These characteristic imprints are in the guise of unique absorption lines and reddening of the spectrum. Occasionally the intervening material is a net emitter of radiation. Thus, quasar spectra hold lots of information about the intergalactic medium (IGM) and also the interstellar medium within the line of sight galaxies. In addition to this, we can use associated absorption systems (absorption systems which are very close to the quasar, or put another way $z_{abs} \simeq z_{em}$) to probe gas in close proximity to QSOs. Studying associated absorption systems (also referred to as clouds) help us in understanding gas inflow/outflow dynamics and the geometrical structure of broad emission line regions.

The spectra of most quasars is populated by emission lines with widths of the order of thousands of $km\ s^{-1}$. These broad emission lines lie on top of a power-law spectrum. Furthermore there may be many narrow absorption lines with widths ranging from tens to a few hundreds of $km\ s^{-1}$. Figure 1 shows a quasar spectra where the quasar continuum and many absorption/emission lines can be seen.A damped Lyman alpha system with redshift $z \sim 2.3$ can also be seen. The absorption features blue-ward of the Lyα emission line are produced by neutral hydrogen in intergalactic clouds whereas heavy elements situated in galactic interstellar clouds are responsible for the red-ward absorption lines. The above mentioned red-ward absorption features can be separated into groups, each with different absorption red-shifts z_{abs}. Each of these groups usually have lines of species such as C IV, N V, O VI, Si IV, Mg II, C II, Si II, Fe II etc. Every group such as this is an associated absorption system (a cloud). The H I lines corresponding to these clouds can be seen if the wavelength range being observed is broad enough. Several such clouds, each with a different red-shift, are often found in quasar spectra. Almost all clouds have absorption redshift z_{abs} smaller than emission red-shift z_{em}. The region on the blue-ward side of the Ly α emission line is commonly referred to as the Ly α forest since most of these lines cannot be attributed to heavy elements are believed to be Ly α at different redshifts.

Many quasars show very broad absorption lines (BALs) with widths of the order

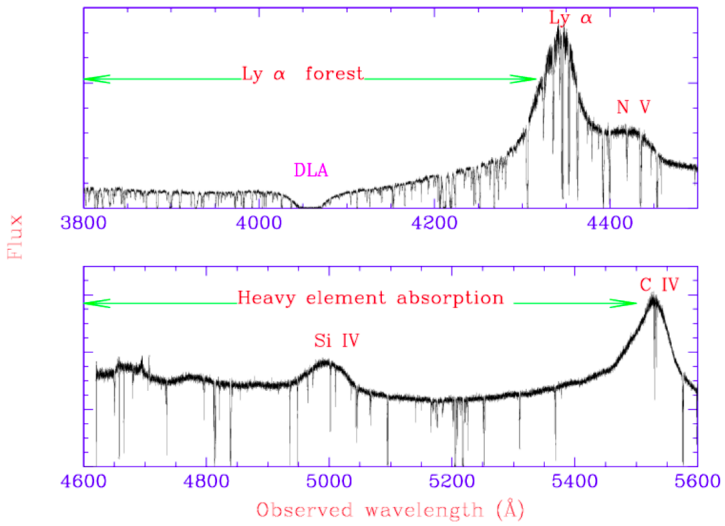

Figure 1: Typical quasar spectrum with $z_{em} \sim 2.6$. Figure from P. Khare (2013)

of thousands of $km\ s^{-1}$. These lines are at redshifts similar to that of the quasars and thus thought to arise from material excreted by the quasar. Sometimes there are lots of narrow absorption lines with redshifts very near to the emission redshift and are also too numerous to be intervening and thus it is likely that most of these are formed by material intrinsic to the quasar. The remaining absorption lines are probably the result of gaseous material, lying along the line of sight, in the IGM or interceding galaxies. Evidence for this claim arises from the following: (see Sargent et al., 1980) (i) Energy source arguments: the observed velocities of the absorbing material,inferred from the difference in emission and absorption redshifts, would require unrealistic amounts of energy, if it was coming from the quasar (ii) difference in the properties of the absorption lines and the quasar, (iii) the distribution of redshifts of the absorption lines resembles a Poisson distribution , and finally (iv) direct observation of intervening galaxies at the redshift of the absorption systems(e.g. Bergeron, 1988; Zwaan et al., 2005).

Absorption line systems in quasar spectra can be used to perform sensitive studies(gas with column densities as small as $10^{11}\ cm^2$ can be measured) on intervening galaxies (without worrying about size, brightness or shape) and the IGM. We have observed quasars with redshifts $z \sim 7$ so galaxies which cover $\sim 94\%$ of the age of universe can be studied with the help of quasar spectra. The study of quasar absorption

line systems has yielded unique information about, and not limited to, ”the large scale structure, structure formation history and nucleosynthesis details, strength, nature and evolution of the UV background radiation field, abundance and nature of dust in the absorbers, quasar outflows, chemical enrichment history of the Universe, cosmic microwave background radiation (CMBR) temperature at high redshifts, variation of the fundamental constants etc.” (P. Khare, 2013).

In the rest of this section I describe the basic concepts that are needed to understand the work that was done in the thesis. I will begin by discussing absorption lines, in particular Voigt profiles and the curve of growth, and then go on to describe line-locking, which is the central part of this work and then end by finally explaining the broad scope of the whole thesis.

2.1 Absorption Line Profiles

A plot of intensity per unit frequency(or wavelength) versus frequency (or wavelength) is called the line profile. In actual physical conditions the line profile is not a delta function centered on the resonance frequency but has a measurable width. There are several causes of this line broadening, both internal and external to the atom, each of which generates its own characteristic profile. Some profiles, for instance, have a wide core and narrow wings (e.g. Gaussian); others have a narrow core and very wide wings (e.g Lorentzian). Analysis of line profiles tells us about the physical conditions, such as the temperature, density and chemical abundances, of the region where the absorption is taking place, which in this case is the region close to the quasar. However, line profile measurement is a tricky task because the accuracy depends heavily on the resolution of the observed spectra. For example it may be the case that two lines are very close together and their profiles are blended together, in this situation determining the exact profile of each line is a complex task where seemingly small errors may lead to erroneous inferences about the system.

”Absorption processes and their signatures imprinted on the spectra of bright background sources (quasars, Gamma-ray burst, etc.) are one of the main sources of information about the physical and chemical properties of intervening systems and of the Intergalactic Matter (IGM). To gain information from absorption lines, it is necessary to model them with some analytical profile whose parameters are related to the physi-

cal properties of the gas from which lines originated"(S. Perrotta, 2016). The radiative transfer equation describes the evolution of the intensity I_ν of the radiation as it propagates through medium,

$$dI_\nu = I_\nu \kappa_\nu dx + j_\nu dx, \tag{1}$$

where dI_ν is the change in the intensity when the wave has traversed an infinitesimal distance dx. κ_ν is the attenuation coefficient at frequency ν, with dimensions of L^{-1}. κ_ν measures the decrease in intensity per unit intensity and distance travelled due to stimulated emission and absorption. So the term $I_\nu \kappa_\nu dx$ gives the net change in intensity due to both of these processes. j_ν gives the emissivity at a frequency ν, with dimensions of power per unit volume unit solid angle per unit frequency. $j_\nu dx$ gives the change in intensity due to spontaneous emission by the material through which the radiation is propagating while traversing a distance dx. Dividing (1) by $\kappa_\nu dx$ we get,

$$\frac{dI_\nu}{\kappa_\nu dx} = -I_\nu + \frac{j_\nu}{\kappa_\nu} \tag{2}$$

$$\frac{dI_\nu}{d\tau_\nu} = -I_\nu + S_\nu(\tau) \tag{3}$$

where $d\tau_\nu = \kappa_\nu dx$ and $S_\nu(\tau) = \frac{j_\nu}{\kappa_\nu}$ are defined as the optical depth and the source function respectively. In this work we are only concerned with absorption lines and so set $S_\nu(\tau) = 0$ to get,

$$I_\nu = I_0 e^{-\tau_\nu} \tag{4}$$

Let us say that we are observing a continuum source occluded by a uniform cloud of gas, using an instrument which has an aperture of solid angle $\Delta\Omega$, and measure the energy flux density F_ν as a function of ν. Integrating (4) over the aperture gives us the flux density as,

$$F_\nu = F_\nu(0) e^{-\tau_\nu} \tag{5}$$

where $F_\nu(0)$ is the original source flux density. We can interpolate over absorption lines to estimate the quasar continuum flux $F_\nu(0)$ over all frequencies. This allows us to evaluate the dimensionless *equivalent width* which is defined as,

$$W_{obs} = \int \frac{d\nu}{\nu_0} \left[1 - \frac{F_\nu}{F_\nu(0)}\right] = \int \frac{d\nu}{\nu_0} (1 - e^{-\tau_\nu}) \tag{6}$$

Another, more intuitive way, to define the equivalent width is in wavelength space,

$$W_{obs}(\lambda) = \int \frac{I_c - I}{I_c} d\lambda = \int d\lambda (1 - e^{-\tau_\nu}) \tag{7}$$

From this it is easy to see that the equivalent width represents the energy that absorption has removed. It is important to note that the integrals in the above two equations extend only over the absorption profile, with the integrand $(1 - e^{-\tau_\nu}) \to 0$ on both edges of the profile.

I will now discuss line broadening mechanisms and how to get the general form of an absorption profile.
(1) **Doppler Broadening** Every atom in a gas is an absorber of radiation and since each atom executes random thermal motion the radiation that each atom experiences in its frame of reference is different due to Doppler shift. We can analytically describe this with a function, by using a Maxwellian distribution, at some temperature T, of atomic velocities, as,

$$\phi(\nu) = \frac{1}{\sqrt{\pi}\Delta\nu_D} e^{-(\frac{\Delta\nu}{\Delta\nu_D})^2} \tag{8}$$

where the *Doppler width* $\Delta\nu_D$ is defined as,

$$\Delta\nu_D = \frac{\nu_0}{c}\sqrt{\frac{2kT}{m}} = \frac{\nu_0}{c} b_{th} \tag{9}$$

where ν_0 is the resonance frequency, $b_{th} = \sqrt{\frac{2kT}{m}}$ is the thermal Doppler parameter and m is the atomic mass of the gas.

(2) **Natural and Pressure Line Broadening** Heisenberg's uncertainty principle states that $\Delta E \Delta t \geq \frac{h}{2\pi}$, which means that an electron cannot have a definite energy for a finite time but energy levels in atoms are quantized so it means that excited states generally have short lifetimes which creates a spread in energy. This spread is intrinsic to every transition. In addition to this there is broadening due to pressure and collisions where de-excitation occurs due to interactions with other atoms in the gas. Both of these mechanisms yield a Lorentzian profile which has the following form,

$$\phi(\nu) = \frac{\Gamma}{4\pi^2} \frac{1}{(\nu - \nu_0)^2 + \left(\frac{\Gamma}{4\pi^2}\right)^2} \tag{10}$$

where the Lorentzian width Γ is given by the sum of natural and collisional line widths. ν_0 is the resonance frequency. The complete line profile is the result of a mixture of

both broadening mechanisms. The central part of the line profile, i.e. frequencies close to resonance, is dominated by the Doppler profile, whereas the Lorentzian profile generated by collisional and natural broadening dominates the edges of the line profile. The convolved Voigt profile can be written as,

$$\Phi(\nu) = \frac{a}{\pi^{3/2}\Delta\nu_D}\int_{-\infty}^{\infty}\frac{e^{-y^2}}{(x-y)^2+a^2}dy \tag{11}$$

where $a = \frac{\Gamma}{4\pi\Delta\nu_D}$ is the ratio of Lorentzian to Doppler width. The dimensionless variable x is given by,

$$x = \frac{\nu-\nu_0}{\Delta\nu_D} = \frac{\lambda-\lambda_0}{\Delta\lambda_D} \tag{12}$$

and gives the distance in frequency (wavelength) from the line center in units of the Doppler frequency (wavelength). The Doppler wavelength is defined as,

$$\Delta\lambda_D = \frac{{\lambda_0}^2}{c}\Delta\nu_D = \frac{\lambda_0}{c}\sqrt{\frac{2kT}{m}} \tag{13}$$

The scattering cross section of the line at resonance is,

$$\sigma_\nu = a_{\nu_0}H(a,x) \tag{14}$$

where H(a, x) is,

$$H(a,x) = \frac{a}{\pi}\int_{-\infty}^{\infty}\frac{e^{-y^2}}{(x-y)^2+a^2}dy \tag{15}$$

and,

$$a_{\nu_0} = \frac{\sqrt{\pi}e^2}{m_e c}\frac{f}{\Delta\nu_D} \tag{16}$$

where f is the oscillator strength. The oscillator strength gives the quantum mechanical correction to the classical absorption/emission rate of a single electron oscillator whose frequency is the same as the transition. Table 1 gives the oscillator strengths of the lines used in this work.

Generally, we can assume the absorbing atoms to have a Maxwellian velocity distribution with mean velocity v_0 in a reference frame O. An atom with velocity v absorbs a photon of frequency ν in O with a cross-section $\sigma(\nu')$, where $\nu' = \nu/(1-v/c)$. Note that the velocity v of the atom is taken as positive when the atom and observer are moving away. The optical depth is,

$$\tau(\nu) = N\frac{1}{\sqrt{\pi}b}\int_{-\infty}^{\infty}\sigma(\nu')e^{-\frac{(\nu-\nu_0)^2}{b^2}}dv \tag{17}$$

Here N is the column density which is defined as the number of the atoms in a cylinder lying along the line of sight with a base of unit area. In this work we will frequently use N_H which is the column density only for hydrogen atoms and can be defined as

$$N_H = \int n_H d\tau \tag{18}$$

where the integration is along the line of sight. n_H is the number of hydrogen atoms per unit volume. Coming back to the derivation, we can define the cross section at any frequency in terms of the cross-section at the resonance frequency as,

$$\sigma_\nu = \sigma_{\nu_0} \phi(\nu) \tag{19}$$

It is important to note that $\phi(\nu)$ should be normalized i.e $\int_{-\infty}^{\infty} \phi(\nu) d\nu = 1$. The expression for σ_{ν_0} is known to be

$$\sigma_{\nu_0} = \frac{\sqrt{\pi} e^2}{m_e c} \frac{f}{\Delta \nu_D} \tag{20}$$

Using eqns 11, 19 and 20 in 17 and representing in terms of wavelength we optical depth.

$$\tau(\lambda) = 1.498 \times 10^{-12} \frac{N f \lambda}{b} H(a,x) \tag{21}$$

For a cloud with uniform density the optical depth at the centre of the cloud is given by

$$\tau_{\nu_0} = 1.498 \times 10^{-15} \frac{f N(cm^{-2}) \lambda_0(\mathring{A})}{b(kms^{-1})}. \tag{22}$$

2.2 Curve Of Growth

The curve of growth is a function that relates the equivalent width of a line (eqn. (7) to its column density. This function depends on the Doppler parameter b as seen in Figure (2). Figure (2) shows a plot between logarithm of the equivalent width (in Å) versus logarithm of column density (in cm^{-2}) for different values of the Doppler parameter (in $km\ s^{-1}$). The curve of growth can be divided into three different regions :

(1) **Linear Part** - Here the column density and the equivalent depth are related linearly. The absorption line is optically thin ($\tau_0 < 0.1$), when the column density is small. Here the Voigt function essentially becomes a Gaussian function. There is no dependence on b here. In this regime the determination of column density (N) from the equivalent width, or vice versa, is easy and reliable.

(2) **Logarithmic Part** - In this regime the equivalent width is weakly dependent on the column density but depends on the temperature (see figure 2). Since a small change in the equivalent width in this regime leads to large change in the column density analysis is very tricky. The equivalent width and optical depth have the following relation at the resonance frequency,

$$\frac{W}{\lambda_0} = 2\frac{b}{c}\sqrt{ln(\tau_0)} \tag{23}$$

(3) **Saturated Part** - In this part the line profiles are characterized by prominent Lorentzian wings. Similar to the linear part, temperature does not differentiate the curve. The column density can be fairly accurately measured using the equivalent width.

Doublets are two closely spaced lines which arise due to fine structure effects. Doublets are often exploited to identify red-shifted systems. In this work I have used the C IV doublet (which has wavelengths 1548.20Å and 1550.7Å) to identify associated absorption systems in quasars. The following scenario illustrates the use of doublets. The following scenario will illustrate how doublets can be used to extract information from the curve of growth. Let (A) be the redder member of the doublet with oscillator strength f_A and (B) be the bluer member with oscillator strength f_B. When the line is optically thin, the ratio of the equivalent widths of the lines will be equal to ratio of their oscillator strength. In this scenario, the column density can be inferred from either line's equivalent width. The temperature of the absorber, however, cannot be determined. As the column density increases the bluer line (line B) will become optically thick first and move on to the logarithmic part of the curve of growth but line A may still be in the first regime.The ratio of the equivalent width will not be given by the ratio of the oscillator strengths when this happens. Now the column density may still be found using the equivalent width of line A and the b-value can be found from the equivalent width of line B.

2.3 Line Locking

Perhaps the most important fact that makes us believe that quasar outflows are accelerated by absorption of light at frequency corresponding to resonance transitions is the presence of absorption features with wavelength difference that is equal to the

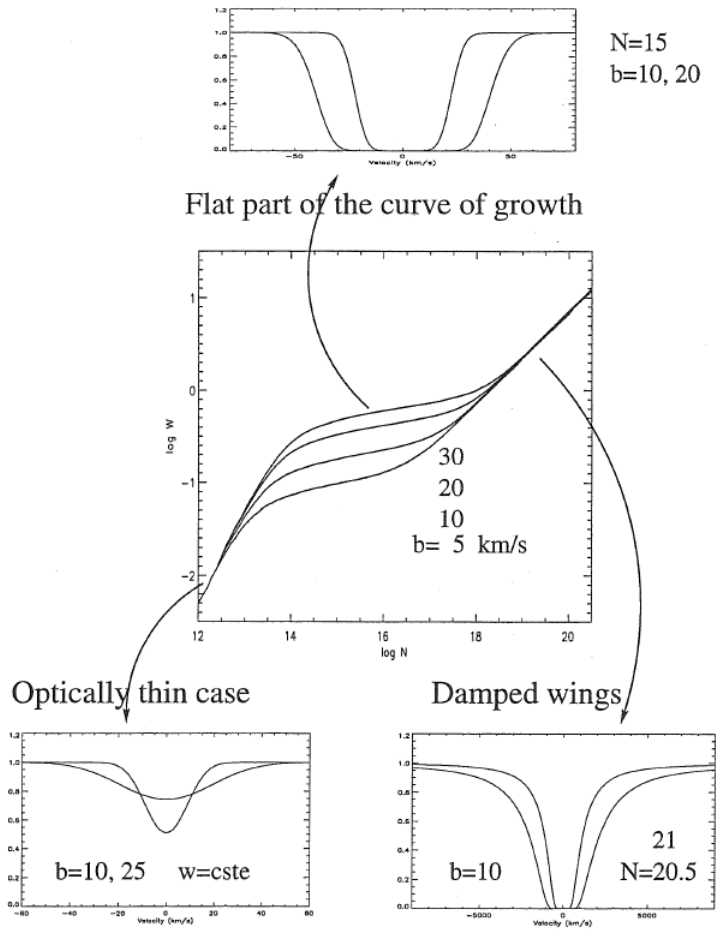

Figure 2: Curve of growth for H I Lyα 1215. Figure from Petitjean (1998).

wavelength difference between resonance line doublets like that of C IV, N V and O VI. Figure 3 shows line locking in the C IV emission lines of Q1511+09 where dark squares, circles and stars show clouds separated by doublet velocity of O VI, C IV and N V respectively.The vertical dotted lines denoted a to j are the 10 clouds observed in the spectra. The top panel is the normalized spectra and the other three plots below show the original spectra and another spectra which is shifted by the doublet splitting of O VI, N V and C IV respectively. Whenever absorption profile troughs coincide in the lower panels the clouds are line locked.

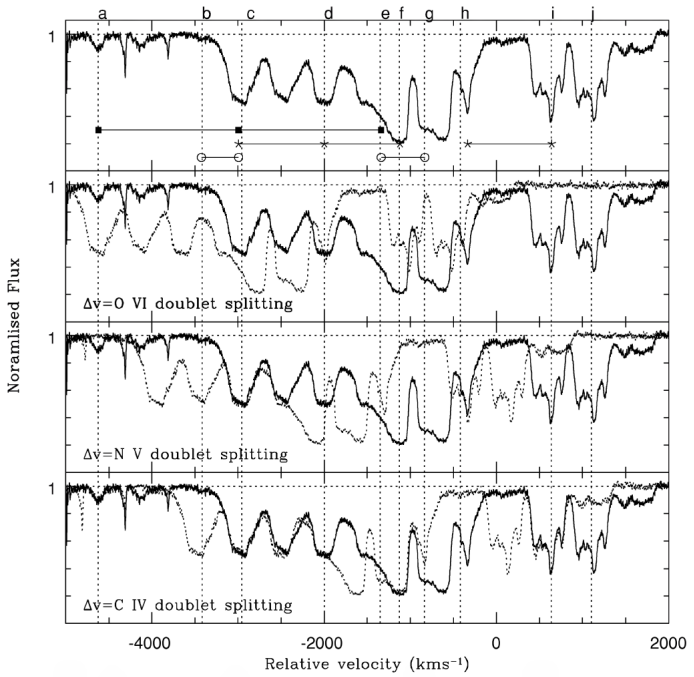

Figure 3: Spectra of Q1511+09 from year 2000 showing line locking. Figure from Srianand (2002).

Suppose there are two clouds near the quasar of which, say cloud 1 is closer to the quasar and cloud 2 is farther away and also there are two lines centered at wavelengths λ_1 and λ_2 (where $\lambda_1 < \lambda_2$) when the cloud is at rest in the quasar atmosphere. When the cloud is moving outward, the lines shift to higher frequency/lower wavelengths in our frame of reference and we have lines centered at λ_1' and λ_2' for cloud 1 (still $\lambda_1' < \lambda_2'$). Farther away from the quasar cloud 2 picks up more velocity and the lines shift further towards lower wavelengths (higher frequency) and we have lines centered around λ_1'' and λ_2''. Now, there may arise a situation where λ_2'' equals λ_1' when the velocity separation between the two clouds produces a Doppler shift equal to the difference in frequency between the two resonance transitions. The following equation tells us what the velocity (v_2) of the outer cloud (cloud 2) should be when the velocity of the inner cloud (cloud 1) is v_1 and the doublet has frequencies ν_1 and ν_2

$$v_2 = v_1 + \frac{\nu_1 - \nu_2}{\nu_1} c \tag{24}$$

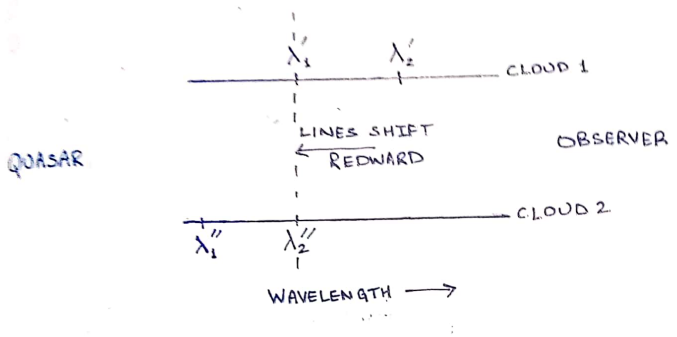

Figure 4: Line Locking

Since the slower cloud is closer to the quasar it absorbs the photons that the faster cloud would have, thus depriving it of acceleration. This effect is called line locking because the clouds will be 'locked in' to these velocities. There are two types of line-locking:

Steady State - In this case the net acceleration of the inner cloud is zero and the acceleration of the outer cloud drops to zero because of line locking. For this either the contribution of the line transition being shadowed should be a significant fraction of the total radiative acceleration or, the net acceleration of the outer cloud should be comparable to the acceleration produced by the line being shadowed. "The double absorption troughs seen in C IV absorption in the case of a few broad absorption line quasi-stellar objects (BALQSOs) suggest such an accelerating mechanism is indeed important in some quasars (Weymann et al., 1991)."(R. Srianand, 2000)

Non-Steady State - In this case locking is based purely on the difference in velocity of the clouds being equal to the doublet velocity separation. The condition of net zero acceleration, and hence balance of inward and outward forces, of the clouds is no longer necessary since absolute velocity is irrelevant. What is required is that the reduction in acceleration of the outer cloud should be equal to the difference in the acceleration's of the clouds before locking. When locked, the velocity of neither clouds is constant but the velocity difference between them is.

2.4 Acceleration

Radiative acceleration is the transfer of momentum carried by photons to the absorbing cloud. This can be through continuum ionization, electron scattering and resonance line absorption. In associated absorption systems we know the clouds are highly ionized, because of the presence of lines of species such as C IV, N V and O VI in the spectra, and thus the effect of continuum absorption is negligible. It is also known that electron scattering contributes appreciably to acceleration only under high electron column densities, i.e., when $N_e \geq 10^{24} cm^2$. Since observations dictate theory, in the range of ionization parameters and electron densities we need to explain the observed column densities of the associated systems, the effect of radiative acceleration due to electron scattering and continuum absorption will be negligible. It is for this reason that we concentrate on radiative acceleration due to resonance line absorption only.

Ionization parameter (U) is defined as the ratio of number of photons emitted from the source per second which are capable of ionizing hydrogen, it is given by,

$$Q = \int \frac{L_\nu}{h\nu} d\nu, \tag{25}$$

where L_ν is the luminosity at frequency ν, and the number of hydrogen atoms in a spherical volume of thickness equal to the distance that light traverses in one second,

$$U = \frac{Q}{4\pi r^2 n_H c}, \tag{26}$$

where Q is defined in eqn. (25), r is the distance from the source, n_H is the number density of hydrogen atoms (both H I and H II). By simple rearrangement we get,

$$r = \left(\frac{Q}{4\pi U n_H c} \right)^{1/2} \tag{27}$$

The gravitational acceleration experienced by the cloud written in terms of U is given as,

$$g = -GM \left(\frac{4\pi U n_H c}{Q} \right) \tag{28}$$

where M is the mass of the central black hole and the force is directed inwards toward the black hole.

The total energy arriving at the cloud at wavelength λ per unit wavelength interval per unit time is,

$$f = L_\lambda \left(\frac{A}{4\pi r^2} \right), \tag{29}$$

where A is the cross-sectional area of the cloud facing the radiation source. The total momentum available for absorption in the incoming radiation per unit wavelength interval per second at wavelength λ is,

$$p(total) = \left(\frac{f}{c}\right) \tag{30}$$

This momentum is transferred to the cloud through line absorption which accelerates it. The radiative acceleration of the cloud due to a absorption of the radiation of a single line transition is,

$$g_r^l = \left(\frac{L_\lambda A}{4\pi r^2 Mc}\right) \int_{line} (1 - e^{\tau_\lambda}) d\lambda = \left(\frac{L_\lambda A U n_H}{MQ}\right) W^l \tag{31}$$

where τ is the optical depth of the line, W^l is the equivalent width of the line and M is the mass of the cloud. Assuming the geometry of the absorbing cloud to be a plane-parallel slab, then

$$g_r^l = \left(\frac{L_\lambda U n_H}{N_H m_H X Q}\right) W^l, \tag{32}$$

where N_H is the total hydrogen column density, m_H mass of a hydrogen atom, and X is the mass fraction of the entire cloud in terms of the mass of a hydrogen atom. The total acceleration of the cloud is obtained by summing over all the transitions. X is assumed to be equal to 1.33 in all of the models. Drag forces due to the medium are ignored.

3 Method

This work can be broadly divided into two parts. The first part is concerned with the modelling of an associated absorption system (henceforth called a cloud) near a quasar. The parameters characterising the properties of the quasar + cloud system i.e. Column density N_H, Hydrogen number density n_H and temperature of the gas in the cloud and the mass of the central black hole were independently varied with little concern if they were physically possible. This was done so that we could first establish if there do exist conditions where steady state line-locking is possible and, if it was, to then make predictions about the conditions under which we would expect to see steady state line-locking. The important results of this part was to get the curve of growth, the column densities of different elements, the acceleration of the cloud and the contribution of individual lines to the total radiative acceleration both as a function of the ionization parameter. In the second part I looked at the spectra of Q1511+09 ($z_{em} = 2.878$) which has been found to show line-locking (R. Srianand, 2002). I looked at the spectra of this quasar for three epochs and tracked 12 different clouds across them. This allowed me to put bounds on the acceleration of individual clouds and also see which clouds remained line-locked. Finally I calculated the column density of individual clouds using the apparent optical depth method (as described in B. Savage, 1991).

3.1 Modelling The Cloud

The aim of this part is to find the acceleration of the cloud as a function of distance from the central super-massive black hole. A lot of parameters have an effect on this function like the elemental composition of the cloud, the spectral energy distribution of the radiation emitted by the quasar, the mass of the black hole, the hydrogen column density of the cloud N_H and the hydrogen number density of the cloud n_H etc. I have tried to vary these parameters as widely as possible as our aim was just to find conditions where steady-state line locking might occur. CLOUDY was an essential part in finding out the properties of the cloud and I will begin by explaining the software.

3.1.1 CLOUDY

Cloudy is designed to make numerical simulations that aid us in understanding complex physical environments starting from first principles. It determines the physical

conditions within a non-equilibrium gas, possibly exposed to an external source of radiation, and predicts the resulting spectrum. This makes it possible to predict many observed quantities by specifying only the properties of the cloud and the radiation field striking it.

Given these assumptions the code will determine the ionization, temperature, and chemical state of a cloud and then predict its spectrum. All of this is done self-consistently with the minimum number of free parameters. The equations of statistical equilibrium, charge conservation, and conservation of energy are solved. These determine the level of ionization, the particle density, the gas kinetic temperature, the chemical state, populations of levels within atoms, and the full spectrum, which often includes hundreds of thousands of lines. A very large number of observables result from a very few free parameters. Often the goal is to determine these free parameters from observations. See section 8 of Ferland (2003) for more.

One starts by creating an input script that specifies the cloud's elemental composition, density, thickness and geometry. In this work all clouds have solar abundances and a plane parallel slab geometry of the cloud. Further, the density and thickness are defined in terms of the proxies hydrogen number density and the hydrogen column density as defined in eqn. (18). The radiation field striking the cloud, often the sole source of heat and ionization, is specified, and other sources of heat can also be included. I used the Matthew-Ferland spectrum, defined by the command 'table AGN', as the only radiation field. The code computes the thermal, ionization, and chemical properties of the cloud, and its observed spectrum. CLOUDY also has the capabilities to run grids and be used as part of a stand-alone program (see section 8 of hazy 2 which can be found in CLOUDY documentation).

It is advised to check if CLOUDY has been installed correctly by running a few basic tests with known results. For this I replicated a result from F. Hamann, 1997. Figures 5 and 6 show relationships between logarithm of ionization fraction with the logarithm of the ionization parameter in optically thin clouds. These plots show us why the relative contribution of different species to radiative acceleration changes with ionization parameter.

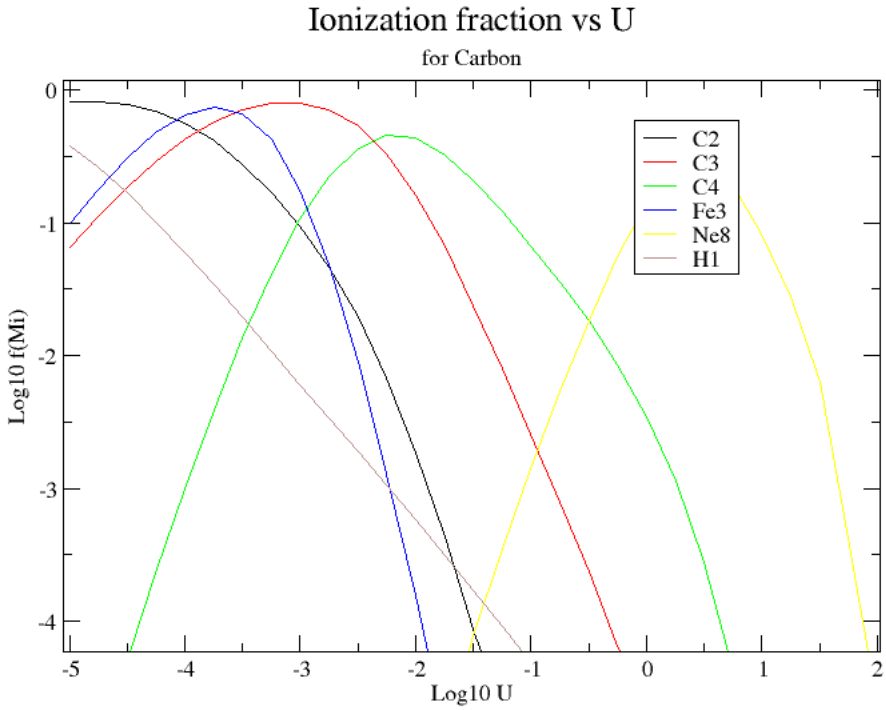

Figure 5: A plot of logarithm of ionization fraction of various species with the logarithm of the ionization parameter

3.1.2 Calculating the acceleration profile

I will now detail how I obtained the net acceleration experienced by a cloud. First I wrote a program that generates the Voigt profile of any line given its column density, oscillator strength, temperature and damping constant. The profile is given by

$$I(\lambda) = I_0(\lambda) exp(-\tau(\lambda)), \tag{33}$$

where $\tau(\lambda)$ is given by eqn. (21). $H(a,x)$ which is given in eqn. (15) was numerically evaluated by Simpson's Method. Here care has to be taken while choosing the step size of the integration depending on the column density of the line. It was found that the step size has to be decreased when the column density is decreased. Also care must be taken while choosing the width of the integration around the resonance frequency. As

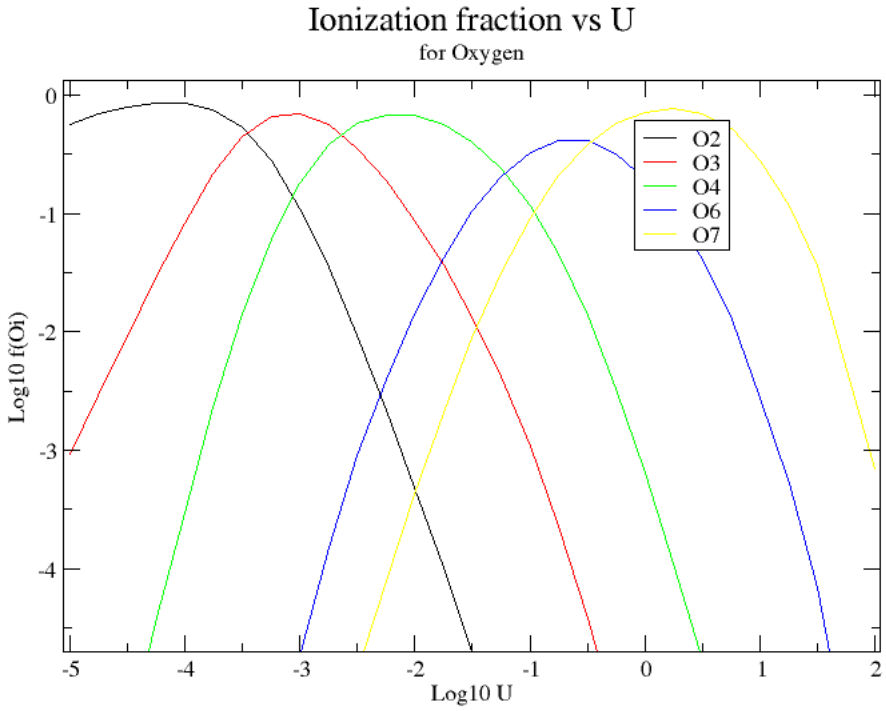

Figure 6: A plot of logarithm of ionization fraction of various species with the logarithm of the ionization parameter

figure (different N profiles) show the Voigt profiles start to develop broad Lorentzian wings as the column density increases above 10^{17} and the range of integration has to be adjusted accordingly. The width of the Voigt profile varies from $\sim 50 kms^{-1}$ when $N \sim 10^{14}$ to $\sim 200 kms^{-1}$ when $N \sim 10^{18}$. The other factors in eqn. (21) are the Doppler parameter b which I have taken to be 10 kms^{-1} and 25 kms^{-1} in my models. The oscillator strength (f) and wavelength (λ) are known. So the only remaining unknown is the column density N for which we use CLOUDY. These Voigt profiles are essential to my project and hence to check that my program does indeed give the correct profiles, I made a curve of growth from them and compared it with those in other sources. My curve of growth for H I is shown in Figure (7). Evidently it is the same as the curve of growth given in Figure (2).

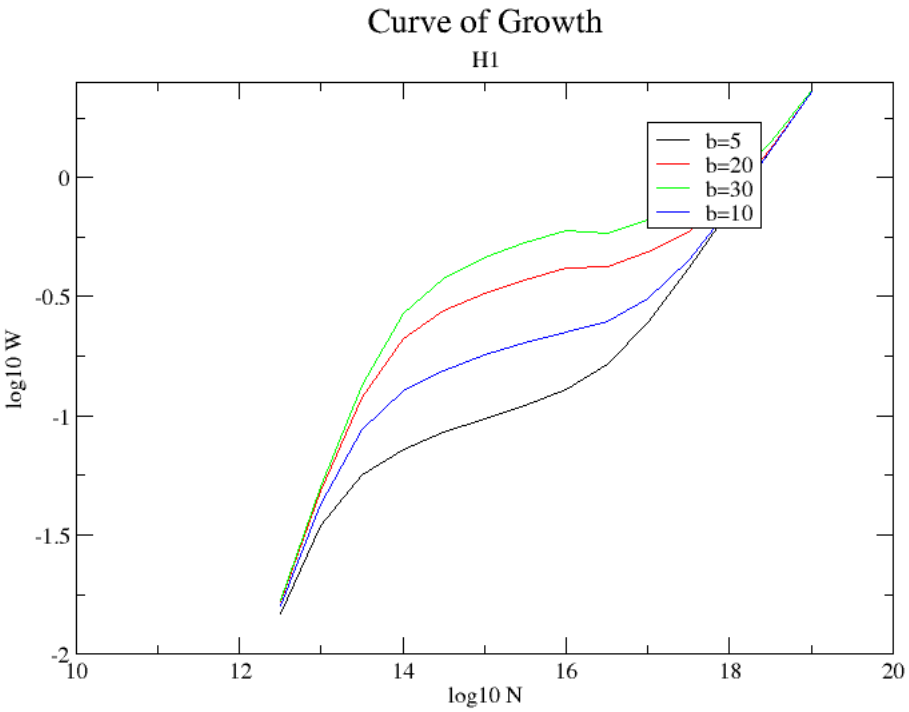

Figure 7: Curve of Growth

I set-up CLOUDY as a stand alone program which takes in as input the hydrogen number density(n_H), cloud geometry (plane parallel slab), incident radiation field (as defined in 'table AGN') and the hydrogen column density (N_H). I then setup a grid with different ionization parameters. The output is the column densities of 11 species which I store to be later used in constructing the line profile as described above. These 11 species whose column densities I have found form the 17 lines that will be radiatively accelerating the cloud. I have listed these lines in Table 1. Equation (32) gives the outward radiative acceleration experienced by the cloud where L_λ is the luminosity at wavelength λ and in this work I have taken it to be given by the Eddington luminosity, which is,

$$L_{edd} = \frac{4\pi GMm_p c}{\sigma_T} = 1.26 \times 10^{31} \left(\frac{M}{M_{sun}} \right) W \tag{34}$$

where M is the mass of the central black hole, M_{sun} is the mass of our sun, m_p is the mass of a proton and σ_T is the Thompson scattering cross-section for an electron. Since our aim is to just find conditions where line-locking can occur I have consider the mass of the central black hole to be 10^7 to 10^9 times the solar mass. Coming back to eqn. (32), X is the mass fraction in terms of the mass of a hydrogen atom and is taken to be equal to 1.33 throughout this work. Q is the number of hydrogen ionizing photons in the incident radiation and following (reference) it is taken to be 10^{54}. The rest of the parameters, i.e. U, n_H and N_H, however, were varied widely.

Species	λ	f	$\gamma(10^8)$
H I	1215.67	0.42	6.26
H I	1025.72	0.08	1.90
C II	1334.53	0.13	2.88
O VI	1037.62	0.07	4.08
C III	977.02	0.76	17.6
C IV	1548.20	0.19	2.64
C IV	1550.78	0.09	2.62
N II	1084	0.11	3.74
N III	989.80	0.12	5.00
N V	1238.82	0.16	3.39
O II	834.47	0.13	2.00
O II	833.33	0.09	2.00
O III	702.33	0.14	2.00
O IV	787.71	0.11	2.00
O VI	1031.93	0.07	4.08

Table 1: Atomic Table with wavelength, oscillator strength (f) and damping constant (γ)of lines used in model

Now we have all the ingredients needed to calculate the net acceleration, which is the sum of the outward radiative acceleration (given by eqn. (32)) and the inward gravitational acceleration given by eqn. (28). This concludes the first part of this project. I

will now move on to how I used observations to corroborate my model.

3.2 Observations

Observations taken by the Ultraviolet and Visible Echelle Spectrograph UVES mounted on the European Southern Observatory (ESO) KUEYEN 8.2-m telescope at the Paranal observatory were used in this work. I have worked on observations taken during three years of the quasar Q1511 +091, which has $z_{em} = 2.878$. The first is from April 04-07, 2000. The wavelength range observed spanned from 3260 Å to 10,000 Å. The observations have a resolution $\sim$ 48,000 and a signal to noise (S/N) ratio $\sim$48. The second observation was taken from April 10-13, 2002 with the observed wavelength range being 4583-6686 Å. The S/N ratio was 22.3 and the resolution was $\sim$ 42,000. The final observation was taken from April 01-03, 2003 with wavelengths being observed from 4583 Å to 6686 Å. The S/N ratio was 26.8 and the resolution was $\sim$ 42,000. The UVES spectrum of Q1511+091 from the year 2000 over the C IV and Si IV emission-line wavelength ranges is shown in the figure below.

3.2.1 Identifying Clouds

Our next task is to identify individual clouds from the spectrum so that we can track them across epochs and find out if they are locked or not. For this I have made use of the C IV doublet which has lines in the rest frame at wavelengths λ_1^0=1548.20 Å and λ_2^0=1550.78 Å. Every cloud with C IV species will form both of these lines at the same redshift and that is what we will exploit. Note that this process of identification can also be done with any other doublet. Suppose that a cloud in the quasar atmosphere has a redshift z then the C IV lines will form at wavelengths,

$$\lambda_1^1 = \lambda_1^0(1+z) \tag{35}$$

and

$$\lambda_2^1 = \lambda_2^0(1+z). \tag{36}$$

Upon dividing the two equation we get,

$$\lambda_1^1 = \left(\frac{\lambda_1^0}{\lambda_2^0}\right)\lambda_2^1 \tag{37}$$

What this equation tells us is that the two lines which are formed by the clouds at an unknown redshift will be related by the above equation. Taking inspiration from this, we superimpose another spectra (in orange) on the original (blue) spectra. The new spectra however has the its wavelength scaled by the factor $\left(\frac{\lambda_1^0}{\lambda_2^0}\right)$. In this superimposed spectra wherever we see absorption troughs in both the original and scaled spectra together we will have identified a cloud. Figures 8, 9 and 10 show how clouds were identified using coinciding absorption troughs. Vertical dotted lines indicate clouds.

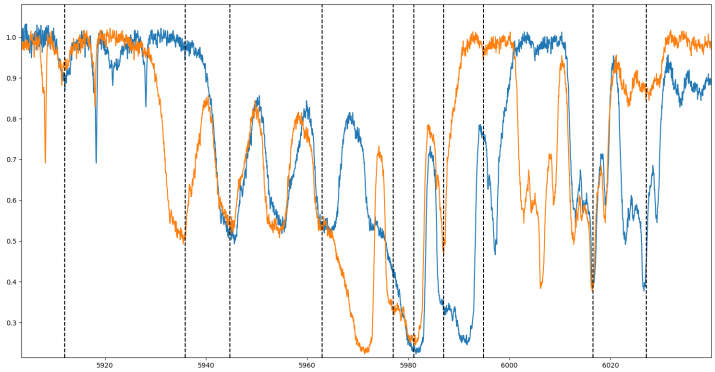

Figure 8: Identifying associated systems: Original spectra is shown in blue and the shifted one in orange. Year 2000.

Now that once the cloud is identified we can use either eqn. (35) or eqn. (36) to find the redshift of the clouds. This approach allows us to identify all the clouds in the quasar atmosphere in one go. Just to check that our identifications are correct I repeated the procedure again but now with Si IV (which has a doublet with wavelengths 1393.76 Angstrom and 1402.77 Angstrom). With this technique 10 clouds were identified in all three of the epochs. Before comparing the redshifts of these clouds across the epochs we have to first bring the observations to a common frame of reference.

3.2.2 Reference Frame Adjustment

Since we are working on observations from three different epochs where the earth was not only rotating about its axis but also revolving around the sun, there is a different

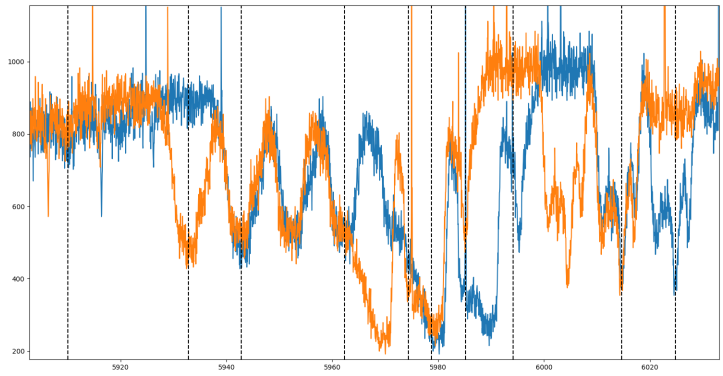

Figure 9: Superposed spectra for year 2002.

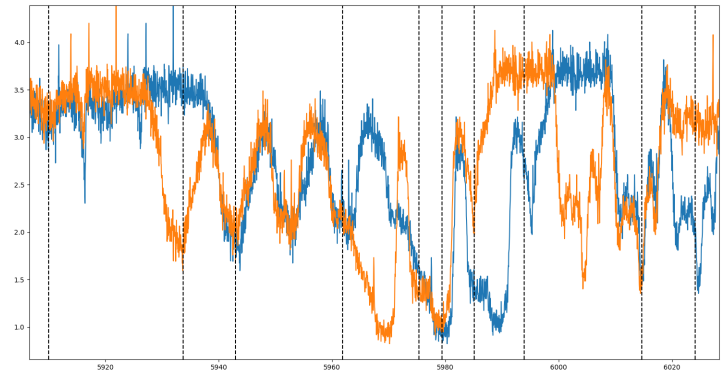

Figure 10: Superposed spectra for year 2003.

relative velocity between the quasar being observed and our telescope. This difference in relative velocity translates into a shift in the wavelength because of Doppler effect. Since in this work we wish to calculate the acceleration of clouds we have to bring all the observations to a common reference frame. To do this I have made use of strong intergalactic lines which can be assumed to be stationary. I have adjusted the 2002 and 2003 spectra to bring it to the reference frame of the 2000 spectra. First of all strong intergalactic lines, clearly visible in all three epochs, were identified. Now since

the intergalactic lines are produced by stationary sources the wavelength should be the same in all epochs, if they are not the same then that must be the result of the earth's motion. Let λ^0 be the wavelength of an intergalactic line in the 2000 spectra and λ^1 be the wavelength of the same line in another epoch then the velocity difference by which the other epoch has to be adjusted by is given by rewriting the Doppler formula as,

$$v = c\left(1 - \frac{\lambda^0}{\lambda^1}\right) \tag{38}$$

where c is the speed of light. This was done with multiple lines to reduce error. I found that to adjust the 2002 epoch we needed to adjust the wavelength by -93.58 kms^{-1} and for the 2003 epoch by -97.93 kms^{-1}. Now we are ready to find the acceleration experienced by the clouds by looking at how much their lines shift by during the epochs.

3.2.3 Apparent Optical Depth Method

The apparent optical depth method is a quick and fairly accurate (especially for high S/N) method to obtain column density from flux profiles, eliminating the need of a full curve of growth analysis or the cumbersome Voigt component fitting (Savage and Sembach, 1991). An absorption line with optical depth $\tau(\lambda)$ will have the following shape in the flux spectrum

$$I(\lambda) = I_0(\lambda) exp[-\tau(\lambda)] \tag{39}$$

where $I_0(\lambda)$ is the continuum intensity and $I(\lambda)$ is the intensity after absorption. This is not however the shape of the line we see in the spectrum because of the finite resolution of observing instrument. The actual observed profile is a convolution of the ideal profile and the instrumental spectral spread function, $\phi_I(\Delta\lambda)$, and given as,

$$I_{obs} = (I_0(\lambda) exp[-\tau(\lambda)]) \otimes \phi_I(\Delta\lambda). \tag{40}$$

The continuum intensity is usually expected to be a slowly varying function over the spread function and so we can write

$$I_{obs} = I_0(\lambda)(exp[-\tau(\lambda)] \otimes \phi_I(\Delta\lambda)). \tag{41}$$

These equations motivate us to define two optical depths

$$\tau(\lambda) = ln\left[\frac{I_0(\lambda)}{I(\lambda)}\right], \tag{42}$$

and

$$\tau_a(\lambda) = ln\left[\frac{I_0(\lambda)}{I_{obs}(\lambda)}\right]. \tag{43}$$

The optical depth $\tau(\lambda)$, as defined in eqn. (42), is called the *true* optical depth since it is derived from the actual line profile without instrumental limitations. The optical depth $\tau_a(\lambda)$, as defined in eqn. (43), is called the *apparent* optical depth as it optical depth we actually observe after instrumental blurring.

Using eqn. (41) we can rewrite eqn. (43) as

$$\tau_a(\lambda) = ln\left[\frac{1}{exp[-\tau(\lambda)] \otimes \phi_I(\Delta\lambda)}\right]. \tag{44}$$

When the instrumental resolution (FWHM[ϕ_I] is high in comparison to the line width (FWHM[line]), $\tau_a(\lambda)$ will be similar to $\tau(\lambda)$ as long as the data has a good signal to noise ratio (S/N$\geq$20) and the continuum intensity is well defined.

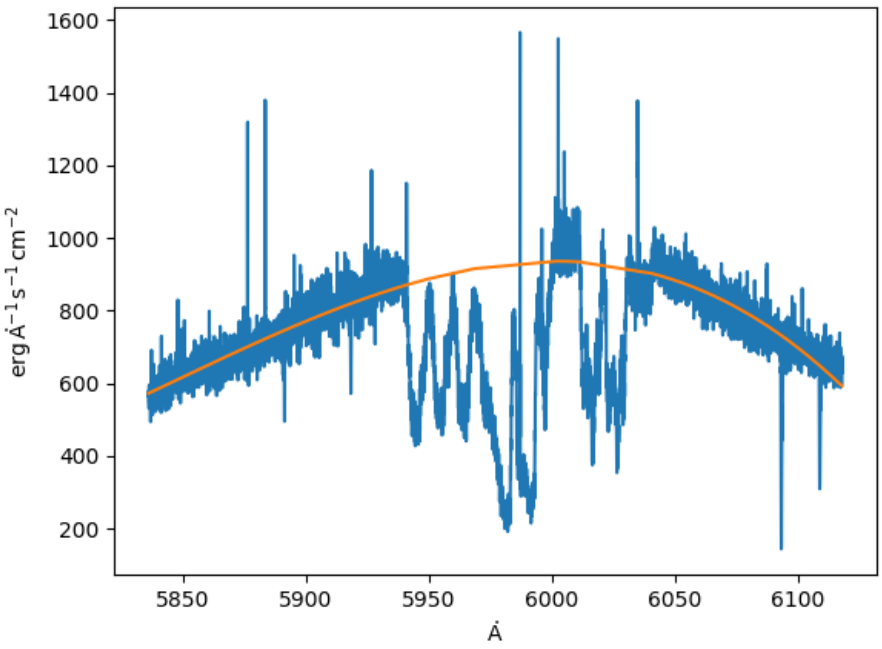

Figure 11: Continuum fitting over spectra of Epoch 2002.

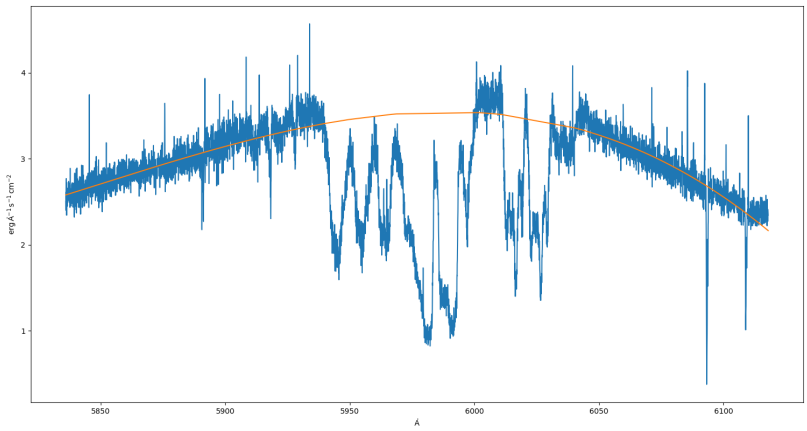

Figure 12: Continuum fitting over spectra of Epoch 2003.

The idea behind the apparent optical depth method is to convert the observed intensity flux profile into an apparent optical depth profile using eqn. (44). Continuum intensity is generally found by interpolation across the absorption trough. Continuum fitting for the spectra of epoch 2002 and 2003 are shown in Figures 11 and 12. Next eqn. (21) is used to relate the optical depth with the column density to get,

$$N_a(v) = 3.768 \times 10^{14} (f\lambda)^{-1} \tau_a(v) cm^{-2} (kms^{-1})^{-1}, \tag{45}$$

where column density is expressed in terms of velocity, f is the oscillator strength and λ is the rest frame wavelength of the transition in angstrom. The total column density is found by,

$$N_a = \int N_a(v) dv \tag{46}$$

where the limits of the integration are the edges of the absorption trough. When doublets with different oscillator strengths are present in a spectra we can use this method find the saturation level of the system by comparing the weaker and stronger lines. This is important because most systems of out concern are affected by partial coverage. The advantages of the apparent optical depth method over the profile fitting and curve of growth methods are: (1) computational ease in calculating column densities and error

estimates; (2) easier to apply when multiple absorption components are present (which is the case for us); (3) significant information line saturation (see Savage and Sembach, 1991, for more detailed discussions).

4 Results and Discussion

In this section I will present and discuss the results of my modelling of clouds in a quasar atmosphere and then look at the spectra from different epochs and show that there is evidence of line-locking in Q1511 +09. Finally I will compare the predictions of the model and the observational evidence to conclude that steady state line locking is unlikely to occur.

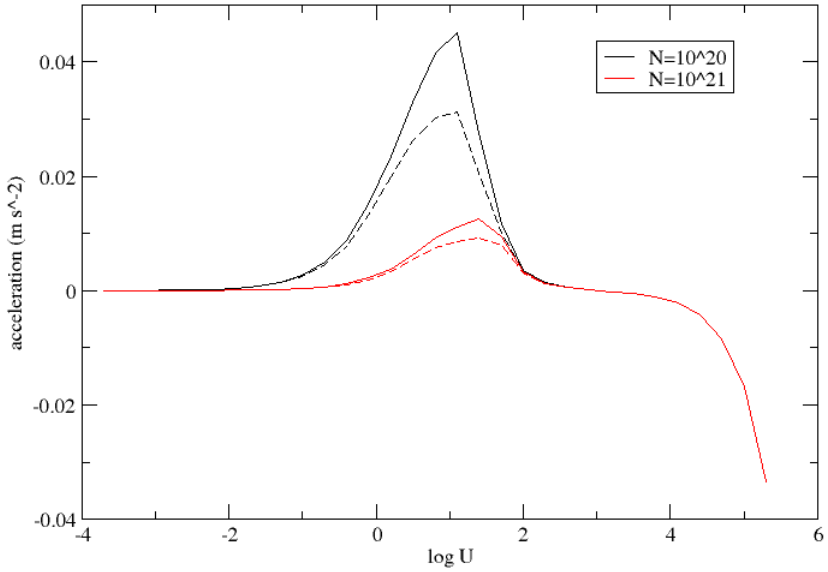

Figure 13: Acceleration vs $\log_{10}$U for two clouds with $N_H = 10^{20}$ and 10^{21}

Figure 13 shows how the acceleration of a cloud varies with the ionization parameter U. The mass of the central black hole used in this model was 10^7 times the solar mass and the number density of hydrogen (n_H) was 10^5 cm^{-3}. The column density for the curve in black is $N_H = 10^{20}$ cm^{-2} and for the curve in red it is $N_H = 10^{21}$ cm^{-2}. Positive acceleration is directed away from the quasar. Since we have fixed Q (ionizing

photon flux) and n_H, the ionization parameter is inversely proportional to the square of the distance from the quasar. On the right edge of Figure 13 we are closer to the quasar and thus the gravitational force dominates. On moving farther away from the quasar we have a sweet spot where the net acceleration drops to zero. This is the region where we expect to see steady state line locking. Moving further away from the quasar (smaller U) we see radiative acceleration dominating and then finally both sources of acceleration become very small. The mass of the black hole only changes the acceleration profile only for high $\log_{10}$U, elsewhere its effect is negligible. For non-steady state line locking the mass of the black hole does not make an appreciable difference.

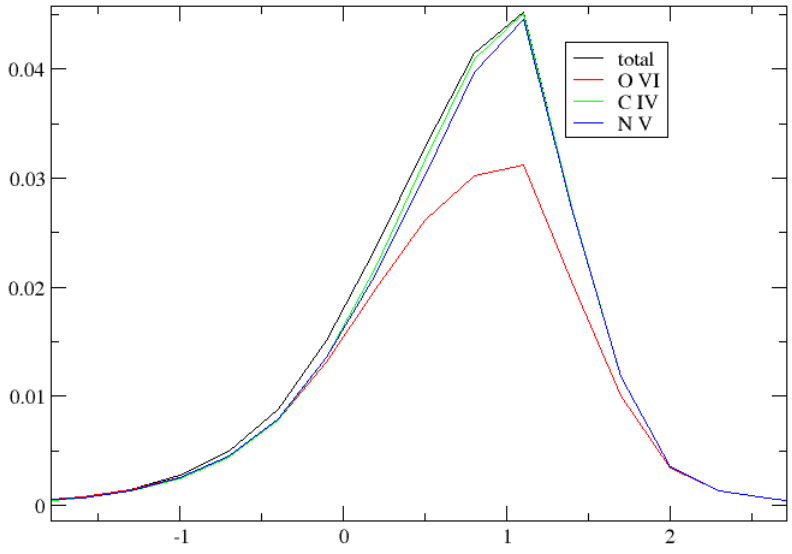

Figure 14: Acceleration profile with O VI, N V and C IV lines shadowed. $N_H = 10^{20}$ and $n_H = 10^5$

The dotted lines in Figure 13 are the acceleration versus ionization parameter curves

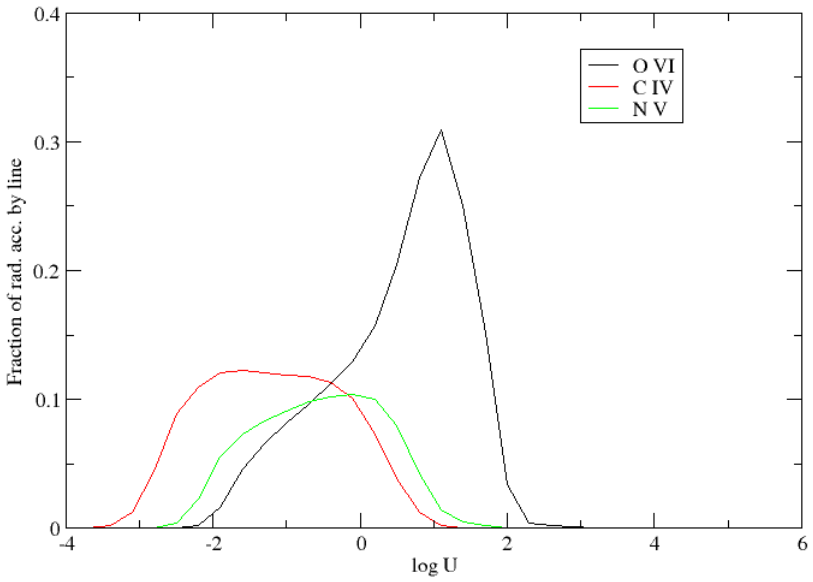

Figure 15: Fraction of radiative acceleration by an individual line versus $\log_{10}$U for $N_H = 10^{20}$ and $n_H = 10^5$

when the radiative acceleration contribution from the O VI line at $\lambda = 1037.62\AA$ is removed. The dotted lines represent the lower limit of acceleration after line locking since I have assumed that the shadowing of the red-ward line is perfect but this is probably not the case in reality. So the profile will lie somewhere in between the solid and dotted line. It is important to note that the contribution of O VI line to radiative acceleration becomes negligible around $\log_{10}\text{U} \sim 2.1$. This spells trouble for the steady state line locking theory because apparently line locking is not needed for zero acceleration at the sweet spot, the acceleration is just small there naturally. If the clouds we observe were to lie in the region between $\log_{10}\text{U} \sim 2.1$ and $\log_{10}\text{U} \sim 3.3$ then we would not observe so many clouds with velocity separation similar to doublet velocity separation (see table 2).

Another possibility is non-steady state line locking where the acceleration of both the

clouds (the one locking and the one getting locked) are equal but non-zero. In this scenario the acceleration of the cloud getting locked (farther from the quasar) is initially higher than the acceleration of the locking cloud (closer to the quasar) but due to the shadowing of a line the outer cloud's acceleration reduces and becomes equal to that of the inner locking cloud. The clouds in this case do not have a fixed velocity but rather a fixed velocity difference. This is clearly possible between $\log_{10}$U$\sim$ 0 and $\log_{10}$U $\sim$ 2 where the contribution of the O VI line is significant (see Figure 13). For this type of locking the locking cloud has a hard condition of $\log_{10}$ U $\geq$1.1 because otherwise the locked cloud will always have lower acceleration. Again looking at Figure 13, the black curve represents the acceleration profile of the locking cloud and the red curve represents the same for the locked cloud. Clearly $\log_{10}$U $\sim$ 1.33 is a great place for the locking cloud to be at since the locked cloud can now have $\log_{10}$U between 1.10 and 0.82.

C IV and N V have very low bearing on the acceleration profile as can be seen from Figure 14 and Figure 15. Figure 15 shows the fraction of radiative acceleration that one line contributes to the total radiative acceleration. The lines being considered are the red-ward lines of doublets, namely O VI with $\lambda = 1037.62\AA$, N V with $\lambda = 1242.80\AA$ and C IV with $\lambda = 1550.78\AA$, since they are the ones that will be shadowed.

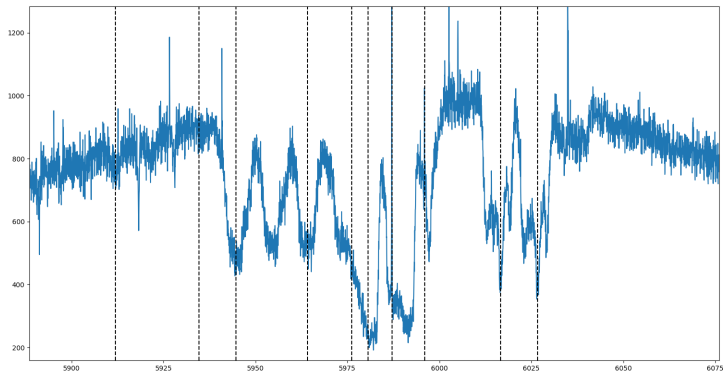

Figure 16: Spectra of Q1511 +09 in year 2000.

For higher column density ($N_H \geq 10^{21}$) the acceleration even without locking be-

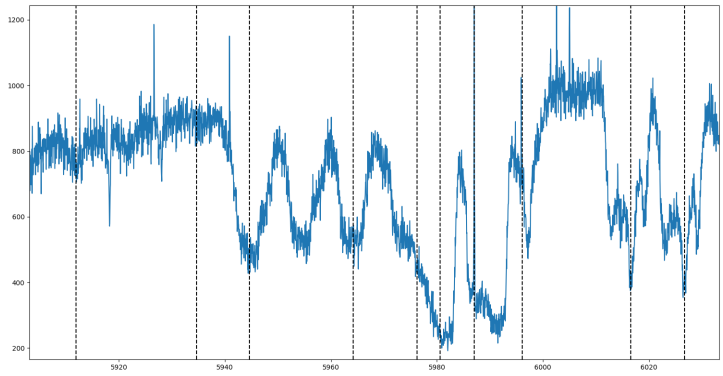

Figure 17: Spectra of Q1511 +09 in year 2002.

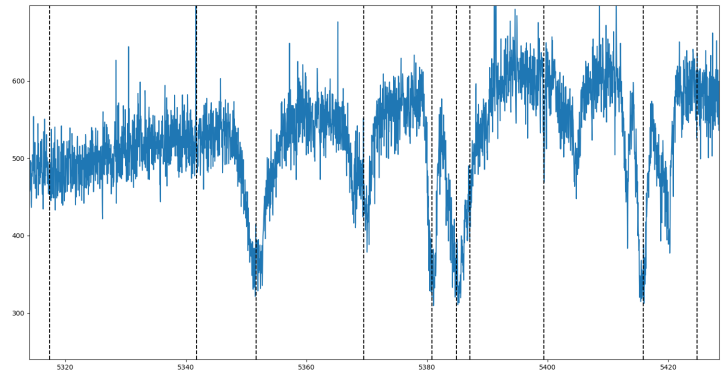

Figure 18: Spectra of Q1511 +09 over Si IV emission lines in year 2002.

comes low enough to account for observations and again we run into the problem of velocity observations matching doublet velocities. I ran similar models to one above for $n_H = 10^5 - 10^9 cm^{-3}$, $N_H = 10^{15} - 10^{22}$ and black hole mass ranging from 10^7 to 10^9 times the mass of the sun and found the model with $n_H = 10^5$ and $N_H = 10^{20} - 10^{21}$ to have the best shot at explaining the observations.

Figures 16, 17 and 19 show the spectrum over the C IV emission lines. Figure

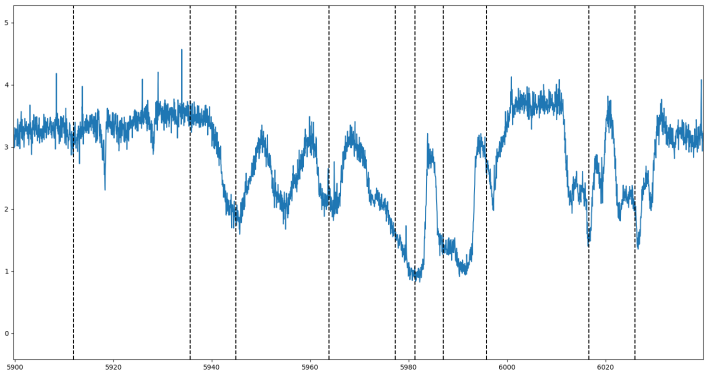

Figure 19: Spectra of Q1511 +09 in year 2003.

18 shows the spectra for epoch 2002 over SI IV emission lines. Dotted lines indicate clouds. The 10 clouds are named 'a' to 'j' from left to right.

Tables 2, 3 and 4 show the actual velocity splittings between the doublets of C IV, N V and O VI, and also the observed splittings between clouds observed in the spectra. Clouds a and c in particular have velocity splittings very similar to the velocity splittings of O VI doublet. This coupled with the fact that O VI lines form a bulk of the outward radiative acceleration points strongly towards the existence of line locking and thus also asserting the proposition that outflows from quasars are primarily driven by line radiation absorption. One point to note is that single clouds are often involved in multiple line lockings. For instance look at component c, it has potential lockings with 4 components namely a, b, d and e. This means that there are many opposing forces acting on each individual cloud and this can potentially explain why velocity separations are not exact matches and also why they are changing. Another possibility to keep in mind is line of sight considerations. All the components need not be, and most probably will not be, directed in the same direction. Thus what we are measuring is the projection of velocities along our line of sight and this can cause measurements to deviate. Still it is undeniable that there is a similarity for the components to be separated by the velocity splittings of doublets.

One fair point to this exercise of claiming that clouds with velocity separation simi-

Doublet	Splitting kms^{-1}	Components	Separation kms^{-1}
C IV	499	b-c	447.12
		e-g	500.58
N V	962	c-d	915.16
		d-f	912.37
		e-h	895.76
O VI	1650	a-c	1648.69
		c-e	1620.71

Table 2: Velocity Splittings Epoch 2000

Doublet	Splitting kms^{-1}	Components	Separation kms^{-1}
C IV	499	b-c	502.13
		e-g	544.17
N V	962	c-d	982.87
		d-f	823.16
		e-h	992.65
O VI	1650	a-c	1650.73
		c-e	1585.28

Table 3: Velocity Splittings Epoch 2002

Doublet	Splitting kms^{-1}	Components	Separation kms^{-1}
C IV	499	b-c	468.30
		e-g	490.06
N V	962	c-d	951.24
		d-f	878.73
		e-h	930.64
O VI	1650	a-c	1666.81
		c-e	1624.65

Table 4: Velocity Splittings Epoch 2003

lar to doublet splittings are line locked is that it might just be a coincidence. R. Srianand et al. (2002) addresses this point by randomly populating the wavelength range with 10 components and seeing how many times the clouds have doublet velocity splittings. They found the probability for two coincides to be 6×10^{-4} after allowing for a mismatch range of 20 $km\ s^{-1}$. Here we observe many more matches so it safe to rule out coincidence. Also we have seen the clouds to be locked across epochs which would not be the case if these clouds were independent.

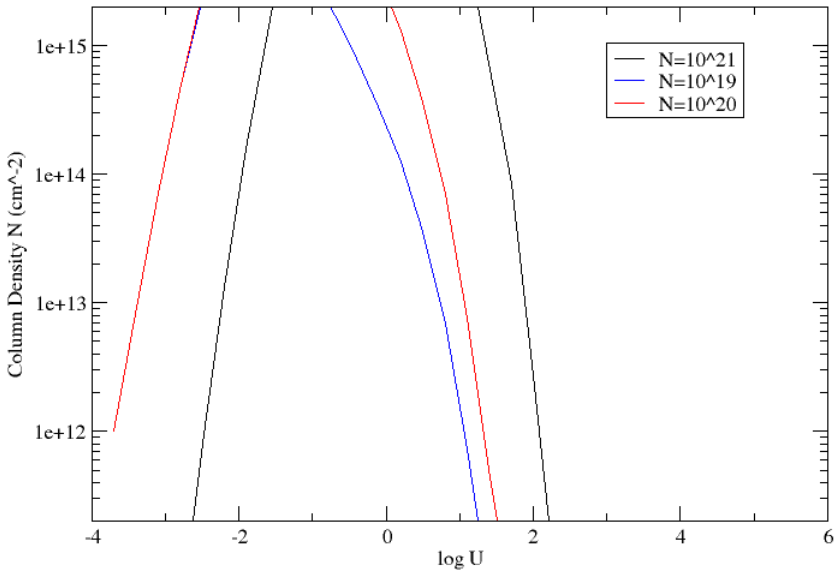

Figure 20: Variation of column density of C IV with $\log_{10}$U for $N_H = 10^{19}, 10^{20}$ and 10^{21}.

Table 5 shows the acceleration of the 10 components averaged over the time period in between observations. The negative acceleration may be the result of line of sight considerations or because of multiple forcings on a single component. The components have acceleration with magnitude between 10^{-3} and 10^{-4} $m\ s^{-2}$ which is close to ac-

celeration profile of $N_H = 10^{21}$ (Figure 13). Table 6 shows the C IV column densities over three epochs for the clouds involved in line locking. The column densities were calculated using the apparent optical depth method. The variability of C IV absorption lines can be seen from the spectra and the column density calculations. This may simply be due to line of sight considerations or because of continuum flux variations. Now observations demand the C IV column densities to range from $\sim 10^{12}$ to 10^{14} cm^{-2}. Figure 20 shows the variation of column density of C IV with the logarithm of U. This figure rules out steady state line locking completely because it would take place when $\log_{10}$U is between 2 and 3 but C IV column density would then be too low to compared to observations. Non-steady line locking, according to the model, would take place for $\log_{10}$U between $\sim$ 1.1 and 2 which puts the predicted C IV column densities very close to the observed values. I was unable to apply the apparent optical method to O VI components because they lie in a highly concentrated part of the spectrum and lines are frequently intertwined.

	Epoch			Acceleration	($\times 10^{-4} m\ s^{-2}$)
Component	2000	2002	2003	00-02	02-03
a	5912.05	5911.93	5911.88	0.957	0.993
b	5935.86	5934.69	5935.62	9.30	-15.3
c	5944.72	5944.64	5944.9	0.635	-4.28
d	5962.91	5964.18	5963.81	-10.05	6.07
e	5977.01	5976.22	5977.27	6.24	-17.18
f	5981.1	5980.59	5981.33	4.02	-12.10
g	5987	5987.08	5987.05	-0.63	0.49
h	5994.91	5996.06	5995.87	-9.05	3.10
i	6016.52	6016.58	6016.6	-0.47	-0.813
j	6027.06	6026.74	6026.04	2.50	11.36

Table 5: Acceleration of clouds across epochs

The two main results of this work are:

(1) Steady state line locking is unlikely because the region where the net acceleration is zero the contribution of doublets to acceleration is insignificant. Non-steady state line locking however, is possible. Congenial conditions for the same present itself with the

2000		2002		2003	
Component	N($\times 10^{12}$)	Component	N($\times 10^{12}$)	Component	N($\times 10^{12}$)
a	6.68	a	3.14	a	3.16
b	1.54	b	2.07	b	4.33
c	112.50	c	131.29	c	143.26
d	96.65	d	114.39	d	105.37
e	67.83	e	84.74	e	102.86
f	142.26	f	203.89	f	186.53
g	95.62	g	91.42	g	106.88

Table 6: Column Density of C IV in clouds from apparent optical depth method

locking cloud having $\log_{10}$U $\sim$ 1.33 and the locked cloud having $\log_{10}$U between 1.10 and 0.82.

(2) O VI plays the dominant role in line-locking dynamics as can be seen from the fractional contribution to radiative acceleration calculations (Figure 15).

5 References

Arav, N., Li, Zhi-Yun, and Begelman, M.C. (1994). Radiative acceleration in outflows from broad absorption line Quasi-Stellar objects. II. Wind Models. ApJ, 432, 62-74.

Bergeron, J., Blades, J. C., Turnshek, D. A., Norman, C. A., (1988), QSO absorption lines: Probing the Universe, Cambridge University Press, p. 275

Hamman, F. (1997). Metal abundances and ionization in quasar intrinsic absorbers. ApJS, 109, 279-305.

Khare, P. (2013). Quasar absorption lines: an overview. Bull. Astr. Soc. India, 41, 41–60.

Lamers, H. Cassinelli, J. (1997). Introduction To Stellar Winds, Cambridge University Press.

Perrotta, S. (2016). Investigating Quasar Outflows at High Redshift. PhD Thesis.

Petitjean, P. (1998). QSO Absorption Line Systems. arXiv.

Sargent, W. L. W., Young, P. J., Boksenberg, A., Tytler, D. (1980). The distribution of Lyman-alpha absorption lines in the spectra of six QSOs: evidence for an intergalactic origin. ApJS, 42, 41-81

Savage, B. D. and Sembach, K. R. (1991a). The analysis of apparent optical depth profiles for interstellar absorption lines. The Astrophysical Journal, 379:245–259.

Srianand, R. (2000). High-resolution study of associated C IV absorption systems in NGC 5548. ApJS, 528, 617

Srianand, R., Petitjean, P., Ledoux, C., and Hazard, C. (2002). A collimated flow driven by radiative pressure from the nucleus of quasar Q1511 + 091. MNRAS, 336, 753-758.

Weymann, R. J., Morris, S. L., Foltz, C. B. and Hewett, P. C. (1991). Comparisons of the emission-lin and continuum properties of broad absorption line and normal Quasi-Stellar Objects. ApJ, 373, 23-53.

Zwaan, M. A., van der Hulst, J. M., Briggs, F. H., Verheijen, M. A. W., Ryan-Weber, E. V. (2005). Reconciling the local galaxy population with damped Lyman cross-sections and metal abundances. MNRAS, 364, 1467-1487.

I used version C17.01 of Cloudy, last described by Ferland et al. (2017)